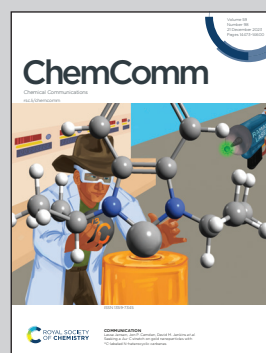Showcasing research from Professor Maeda's laboratory, Department of Chemistry, Tokyo Gakugei University, Tokyo, Japan and Professor Ehara's laboratory, Research Center for Computational Science, Institute for Molecular Science, Aichi, Japan

Recent progress in controlling the photoluminescence properties of single-walled carbon nanotubes by oxidation and alkylation

Functionalization of single walled carbon nanotubes (SWCNTs) has proven to be effective in tuning the photoluminescence (PL) based on selected reaction techniques and molecular structures. This review delves into the latest developments in tailoring the PL through oxidation and alkylation.

As featured in:

See Yutaka Maeda *et al.*, *Chem. Commun.*, 2023, **59**, 14497.

ROYAL SOCIETY OF **CHEMISTRY**

rsc.li/chemcomm

Registered charity number: 207890

FEATURE ARTICLE

Check for updates

Recent progress in controlling the photoluminescence properties of single-walled carbon nanotubes by oxidation and alkylation

Yutaka Maeda, [iD] *[a] Pei Zhao [iD] [b] and Masahiro Ehara [iD] [b]

The functionalization of single-walled carbon nanotubes (SWCNTs) has received considerable attention in the last decade since highly efficient near-infrared photoluminescence (PL) has been observed to be red-shifted compared with the intrinsic PL peak of pristine SWCNTs. The PL wavelength has been manipulated using arylation reactions with aryldiazonium salts and aryl halides. Additionally, simple oxidation and alkylation reactions have proven effective in extensively adjusting the PL wavelength, with the resulting PL efficiency varying based on the chosen reaction techniques and molecular structures. This review discusses the latest developments in tailoring the PL attributes of SWCNTs by oxidation and alkylation processes. (6,5) SWCNTs exhibit intrinsic emission at 980 nm, and the PL wavelength can be controlled in the range of 1100–1320 nm by chemical modification. In addition, recent developments in chiral separation techniques have increased our understanding of the control of the PL wavelength, extending to the selection of excitation and emission wavelengths, by chemical modification of SWCNTs with different chiral indices.

Introduction

Single-walled carbon nanotubes (SWCNTs) with a tubular graphene structure have attracted significant attention owing to their remarkable mechanical strength and distinct electronic and optical properties.[1,2] The chiral index (*n*,*m*) represents the vector orientation of the graphene sheet and defines the

[a] *Department of Chemistry, Tokyo Gakugei University, Tokyo 184-8501, Japan.*
  E-mail: ymaeda@u-gakugei.ac.jp
[b] *Research Center for Computational Science, Institute for Molecular Science,*
  Okazaki 444-8585, Japan

Yutaka Maeda received his PhD degree from Niigata University in 2001 under the guidance of Prof. Takeshi Akasaka. After working as a postdoctoral fellow at the University of Tsukuba, he moved to the Tokyo Gakugei University as an assistant at the Department of Chemistry in 2002. He was a PRESTO researcher at the Japan Science and Technology (JST) Agency between 2006 and 2010. He was promoted to associate professor and professor of chemistry in 2008 and 2020, respectively. His research interests include the organic chemistry of nanocarbon materials, such as fullerenes and carbon nanotubes.

Yutaka Maeda

Pei Zhao received her PhD from Xi'an Jiaotong University in 2018, supervised by Prof. Xiang Zhao. She began the postdoctoral research in the group of Prof. Masahiro Ehara at the Institute for Molecular Science, and became a research assistant professor in 2022. Her research focuses on investigating the electronic structures of complex systems to understand their bonding features, optical properties and catalytic activities using theoretical calculations.

Pei Zhao

Feature Article

structure of SWCNTs. SWCNTs with $\mathrm{mod}(n-m,3) = 0$ exhibit a metallic band structure, while those with $\mathrm{mod}(n-m,3) \neq 0$ display a semiconducting band structure (Fig. 1a).[3] The band gap energy of semiconducting SWCNTs is inversely proportional to their diameter. To harness the electronic and optical properties of SWCNTs, selecting SWCNTs with an appropriate chiral index is crucial, which can be characterized based on absorption[4] and Raman spectral analysis.[5] In 2002, Weisman *et al.* reported the photoluminescence (PL) of semiconducting SWCNTs in the near-infrared (NIR) region. This was observed by exfoliating bundled SWCNTs, a process aimed at minimizing the interactions between the SWCNTs.[4,6] Exfoliation was achieved by sonication in a D_2O solution containing a surfactant, followed by ultracentrifugation. To observe the PL spectra of semiconducting SWCNTs, they must be excited at the second-lowest excitation energy (E_{22}) owing to the minimal Stokes shift originating from their rigid tubular structures. Fig. 1b and c displays the absorption spectra and contour plots for the excitation and emission wavelengths of the as-prepared HiPco SWCNTs,[7] respectively. These PL peaks can be assigned to specific chiral indices based on their excitation and emission wavelengths, as detailed in Table 1. Various types of dispersant reagents have been investigated, including surfactants, π-conjugated compounds, amine, and polymers. It was reported that chiral-index-selective dispersion and PL wavelength shifts[8–13] occur depending on the solvents and dispersant reagents; therefore, the dispersion conditions are important for chiral index assignment and for evaluating the proportions of the different chiral SWCNTs in a mixture.

The PL spectra of SWCNTs are promising as NIR light sources, with applications in bioimaging[14] and room-temperature single-photon emission.[15] Imaging technologies, such as computed tomography, magnetic resonance imaging, and ultrasound, have been widely employed in diagnostic and therapeutic applications. Optical imaging enables real-time measurements using NIR light for enhanced sensitivity and deep-tissue observation.[16,17] Emitting light in transparent
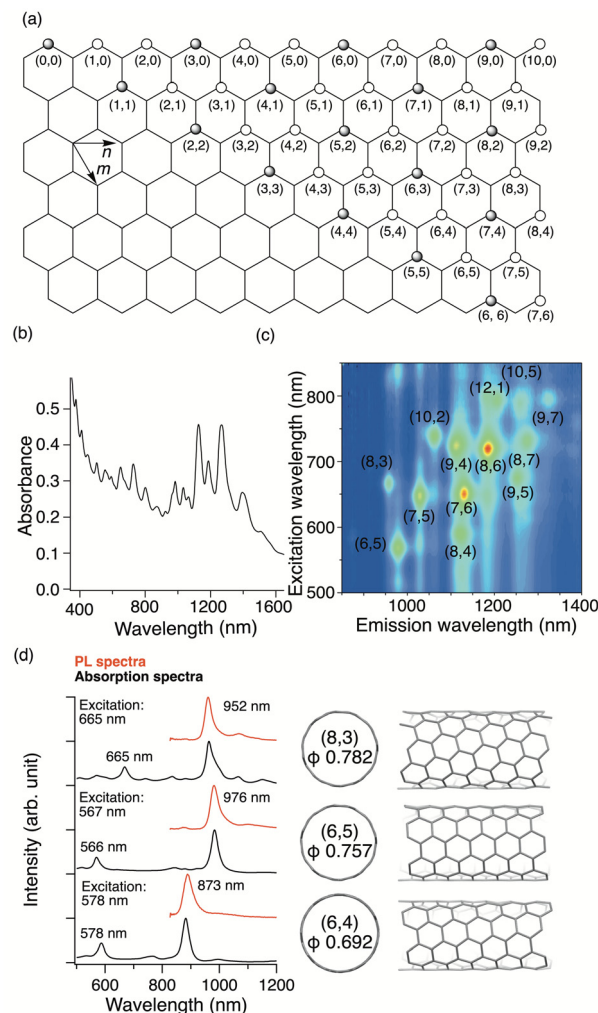

Fig. 1 (a) Development view of SWCNTs with its chiral index highlighted. SWCNT in which the (0,0) and (n,m) carbon atoms coincide are denoted as (n,m) SWCNT. (b) Absorption and (c) PL spectra of HiPco SWCNTs dispersed in D_2O solution containing 1 wt% sodium cholate. (d) Absorption and PL spectra along with structures of (6,4), (6,5), and (8,3) SWCNTs.

Masahiro Ehara received his PhD from Kyoto University in 1993. After the postdoctoral career at the Fukui Institute for Fundamental Chemistry and Heidelberg University, he became an assistant professor and associate professor at Kyoto University. Since 2008, he has been a professor at the Institute for Molecular Science and Research Center for Computational Science. His research interests involve the theoretical and computational chemistry of complex systems including photo-functional systems and heterogeneous catalysts.

Masahiro Ehara

Table 1 Spectral data and assignments for SWCNTs

Chiral index	Diameter (nm)[54]	E_{22} wavelength (nm)[54]	E_{11} wavelength (nm)[54]	RBM (cm^{-1})
(5,4)	0.620	483	835	373[4]
(6,4)	0.692	578	873	337[4]
(6,5)	0.757	566	976	309[4]
(7,3)	0.706	505	992	330[55]
(7,5)	0.829	645	1024	283[4]
(7,6)	0.895	648	1120	264[4]
(8,3)	0.782	665	952	297[4]
(8,4)	0.840	589	1111	280[55]
(8,6)	0.966	718	1173	246[55]
(9,4)	0.916	722	1101	317[56]
(9,5)	0.976	672	1241	242[55]
(9,7)	1.103	793	1322	215[4]
(10,2)	0.884	737	1053	265[4]
(10,5)	1.050	788	1249	226[4]

windows (NIR-I: 750–900 nm, NIR-II: 1100–1700 nm) decreases autofluorescence and phototoxicity, offering increased

signal-to-background ratios and deeper penetration. These advantages stem from the ability to select an appropriate SWCNT chiral index for specific excitation and emission wavelengths. However, the requirement for E_{22} excitation in the visible light region for E_{11} PL observation owing to the small Stokes shift (Fig. 1d) and low PL quantum yield of the E_{11} PL[18,19] hinders their practical applications.

In 2010, Weisman *et al.* reported that oxidized SWCNTs exhibited a new PL peak in a longer wavelength region than the E_{11} PL peak, which was excited at the E_{11} energy (Fig. 2).[20] Moreover, the PL efficiency was modulated by the functionalization degree, reaching a value at least 18-fold greater than that of the pristine (6,5) SWCNTs.[21] These pioneering studies spurred research on manipulating the NIR PL characteristics of SWCNTs by chemical functionalization. Recent studies have investigated the effect of chemical functionalization on the PL properties of SWCNTs with different chiral indices and methods for controlling the PL wavelength. Controlling the PL characteristics of SWCNTs using arylation reactions and related theoretical analysis,[22,23] involving diazonium chemistry,[24–29] aniline derivatives,[30–33] aryl halides,[31,34,35] *etc.*,[36] has also been extensively studied to increase the PL efficiency and tune the PL wavelength. Numerous comprehensive review papers[37–41] have spotlighted these outstanding contributions. Using arylation reactions, the PL wavelength of (6,5) SWCNTs can be extensively tuned by electronic effects,[24,34,42] steric effects of substituents,[43–48] and the number of reactive sites.[26,34,42,47,49–52] These findings offer deep insights into the factors governing the PL attributes. This feature article highlights seminal and recent advancements in controlling the NIR PL wavelength of SWCNTs through oxidation and alkylation reactions.

PL controlled by oxidation of SWCNTs

In 2010, Weisman *et al.* applied photochemical oxidation of fullerene C_{60} using ozone to oxidize SWCNTs dispersed in a D_2O solution (Fig. 2, Scheme 1).[20] Their work revealed that as the intrinsic E_{11} PL peak intensity decreased, a new PL peak emerged at wavelengths 10–15% longer than the E_{11} PL wavelength for 10 distinct chiral SWCNTs under this photo-oxidation. Specifically, oxidized (6,5) SWCNTs exhibited a new PL peak at 1120 nm (E_{11}^* PL). The E_{11}^* PL intensity initially increased and then decreased as the reaction proceeded. To ensure reproducibility, minimal ozone exposure and the use of sodium tridecylbenzenesulfonate (STBS) proved to be effective. Although weak oxidants like H_2O_2 and K_2CrO_4 were less effective, they still resulted in the emergence of a new PL peak. The origin of this post-photoreaction peak was verified by theoretical calculations of model compounds, including ether- and epoxide-type addition products. Calculations using a semiempirical model of the highest occupied molecular orbital (HOMO) and the lowest unoccupied molecular orbital (LUMO) indicated a reduced HOMO–LUMO gap due to oxidation. Therefore, following light absorption, the generated exciton was captured by the lowered potential at the functionalization site and emitted at a longer wavelength than the inherent E_{11} PL wavelength. Functionalization offers several benefits for NIR emission in SWCNTs: (1) The E_{11}^* PL peak can be excited by E_{11} absorption in the NIR region, which is more absorptive than E_{22} absorption in the visible region. (2) The excitation efficiency of the E_{11}^* PL surpasses that of E_{11} PL efficiency in pristine SWCNTs, varying with the functionalization degree. (3) Excitation at the E_{11} energy and the emergence of E_{11}^* PL enhance the
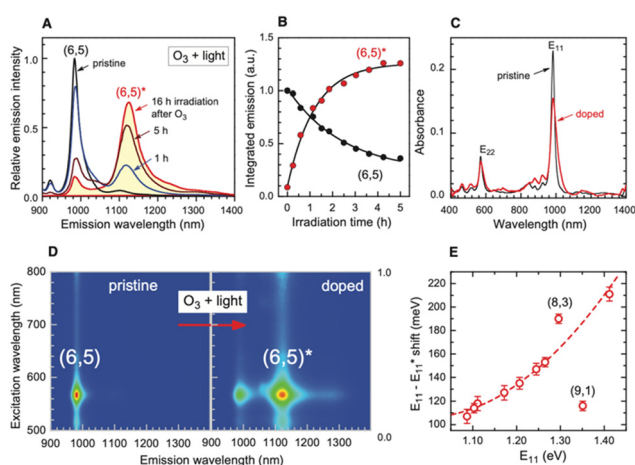

Fig. 2 (A) PL spectral changes in (6,5)-enriched SWCNT dispersion exposed to ozone and light. (B) Spectrally integrated emission under the (6,5) main band (black) and side band (red) *versus* irradiation time using a desk lamp. (C) Absorption spectra of the SWCNT sample before and after treatment with ozone and light. (D) PL excitation–emission contour plots from the (6,5)-enriched sample before (black) and after treatment (red). (E) Measured photon energy differences between the unshifted and shifted PL peaks of 10 different bulk (n,m) species as a function of the unshifted emission energy. Reprinted with permission from ref. 20. Copyright 2010 American Association for the Advancement of Science.
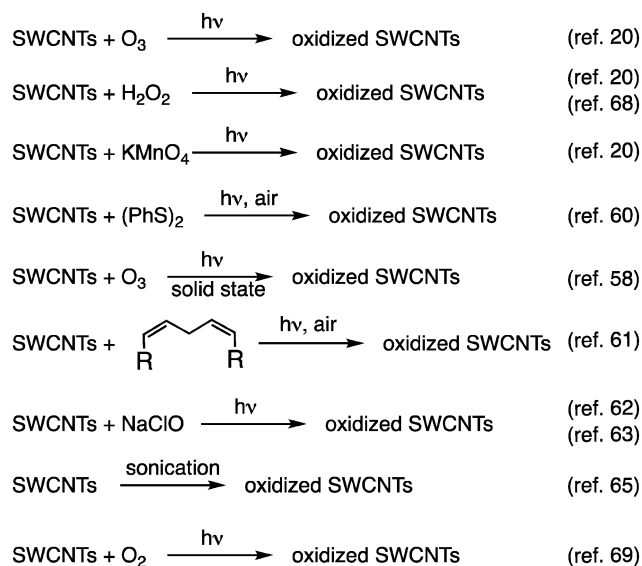
Scheme 1 Oxidation reactions of SWCNTs for controlling NIR PL characteristics.

NIR PL efficiency and minimize autofluorescence and photo-toxicity, facilitating deep bioimaging. (4) Additionally, the new PL from functionalization has an extended lifetime, and upconversion PL (UCPL) at E_{11} can be observed when excited at the wavelength of the new PL peak.[49,53]

In 2014, Htoon et al. conducted low-temperature PL measurements of oxidized (6,5) SWCNTs prepared by photooxidation with ozone.[57] Under certain conditions, multiple sharp PL peaks were observed at wavelengths of 40–300 nm, which are longer than the E_{11} PL wavelength. By comparing these wavelengths with electron transition energies from time-dependent (TD) density functional theory (DFT) calculations, these PL peaks were assigned to ether- and epoxide-type oxidized SWCNTs. These results suggest that the PL wavelength can be manipulated by altering the structure of the oxidized SWCNTs. The local structure of oxidized SWCNTs and their transition energies have been widely employed to determine the structure of oxidized SWCNTs from experimentally observed PL wavelengths. In 2018, Okazaki et al. observed a new broad PL peak at 1280 nm with a shoulder at 1160 nm in (6,5) SWCNTs after the solid-state photoreaction of SWCNTs with ozone.[58] The intensity ratio of these peaks was $1:1.3$. These new PL peaks were attributed to ether- and epoxide-type oxidized SWCNTs based on the experimental and theoretical findings reported by Ma et al. (Fig. 3).[57] High-resolution images were obtained in bioimaging experiments using oxidized SWCNTs.[58] Another solid-state functionalization to control the PL characteristics, an arylation reaction, was reported by Kato et al.[35]
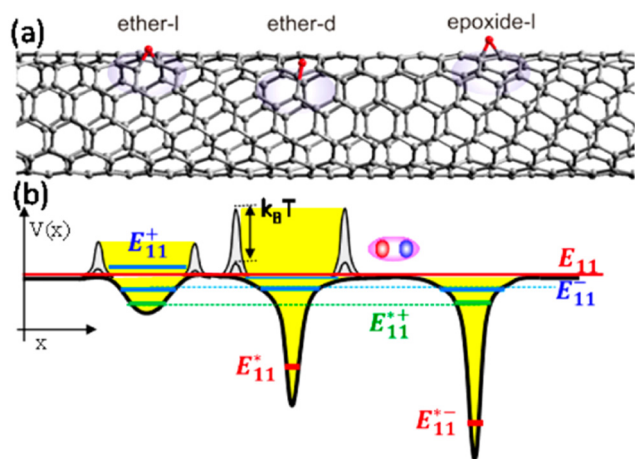

Fig. 3 (a) Structure of ether-l (left), ether-d (center), and epoxide-l (right) adducts on a segment of the (6,5) SWCNTs. (b) Schematic of the potential profile along the length of the tube showing potential traps created by the ether-l (left), ether-d (center), and epoxide-l (right) adducts. The deep trap states and states that result from the brightening of the dark states are marked with brown and blue lines, respectively. The bright exciton state of the undoped tube is represented by a red line. The fluctuation of small potential barriers in the vicinity of the trap site leads to the fluctuation of the exciton trapping efficiency and negatively correlated PL intensity fluctuations between E and dopant related emissions (i.e., E^* and E^-). Reprinted with permission from ref. 57. Copyright 2014 American Chemical Society.

In 2013, Maeda et al. applied the oxidation reaction of fullerene C_{60} using sulfide[59] to develop the photochemical oxidation of SWCNTs using diphenyldisulfide in tetrahydrofuran (THF).[60] Similar to the photoreaction with ozone,[20] a new PL peak emerged at 1120 nm from the (6,5) SWCNTs. This reaction exhibited a higher selectivity toward metallic and small-diameter SWCNTs. Similar to the use of low concentrations of ozone and STBS in ozone oxidation to control SWCNT reactivity, the reduced reactivity of the semiconducting SWCNTs effectively regulated the functionalization degree, leading to the emergence of E_{11}^* PL at an appropriate intensity. For fullerene C_{60}, an efficient singlet oxygen ($^1O_2$) sensitizer, a persulfoxide intermediate, is generated by the reaction between $^1O_2$ and sulfide, which subsequently reacts with C_{60} to produce fullerene epoxide ($C_{60}O$). However, SWCNTs were oxidized only with disulfide and not sulfide. Photo-induced electron transfer affording a nucleophilic oxygen transfer intermediate, thiopersulfinate, was proposed. This was supported by detecting a radical ion intermediate via low-temperature electron paramagnetic resonance and laser flash photolysis experiments. The nucleophilic reactivity of the thiopersulfinate intermediate is consistent with its higher reactivity toward metallic SWCNTs. A reaction that is less reactive to semiconducting SWCNTs enables effective control of the PL intensity, making functionalization degree control more straightforward.

In 2017, Star et al. demonstrated the photochemical oxidation of SWCNTs using polyunsaturated fatty acids (PUFAs), revealing a new PL peak at 1120 nm for (6,5) SWCNTs.[61] A control experiment and characterization suggested that linoleic acid (LA) is oxidized to form lipid hydroperoxides (LA–OOH). LA–OOH then reacts with the photoexcited SWCNTs to form ether-type oxidation products. The photoreaction was more efficient when the photoirradiation wavelength matched the resonance wavelength of SWCNTs. Moreover, the type and concentration of surfactants strongly influenced the reaction efficiency.

In 2019, Lin et al. reported the photochemical oxidation reaction of SWCNTs using hypochlorite, resulting in a new PL peak at 1126 nm for (6,5) SWCNTs.[62] The research suggested that the photolysis of hypochlorite generated reactive oxygen which oxidized SWCNTs. The reaction efficiency was strongly dependent on the surfactant type and concentration. Eremin et al. reported that mild UV exposure achieved bright emissions.[63] They proposed that a milder reaction may promote a uniform oxidation reaction to improve the PL efficiency. For in vivo imaging, a high-throughput flow reactor was developed, capable of generating approximately 0.3 mg h^{-1} oxidized SWCNTs.[62] Moreover, high-contrast bioimaging was achieved using a minimal amount of oxidized SWCNTs (100 ng of SWCNTs per mouse). The degradation of SWCNTs in wastewater using hypochlorite is accelerated depending on the treatment conditions, including hypochlorite concentration, reaction temperature, and pH values.[64] This underscores the importance of precise reactions for controlling the PL properties utilizing hypochlorite as an oxidant.

Sonication is the predominant method employed for dispersing SWCNTs in solution. While preparing SWCNT dispersions for PL analysis, a new PL peak at 1120 nm for (6,5) SWCNTs emerged with an increase in sonication time.[65] Sonication in an aqueous solution containing SDBS is commonly utilized to prepare well-dispersed SWCNTs for solution-phase analysis.[66] Such alterations in PL properties were absent in SWCNTs using other surfactants, such as sodium dodecyl sulfate (SDS) and sodium cholate (SC). This oxidation was observed at low SWCNT concentrations, indicating the limited efficiency of the reaction. Surfactants can be decomposed by ultrasonic irradiation. Hydrogen peroxide and hydroxyl radicals are generated from water by ultrasonic irradiation, which react with the surfactant and decompose them.[67] This reaction is accelerated in the presence of metal ions. Aligning with these findings, the characteristic PL alterations of SWCNTs upon sonication were accelerated in the presence of a metal catalyst and inhibited in the presence of a radical inhibitor. The reaction efficiency increased under an Ar atmosphere with 1-butanol, indicating that dissolved oxygen impeded the reaction. These results suggest that the sonochemical oxidation of SWCNTs involves the generation of radical species, such as hydroxyl radicals.

Kataura *et al.* reported gel chromatographic separation of pristine SWCNTs. They discovered that the separated (5,4) and (6,4) SWCNTs exhibited new PL peaks corresponding to oxidized SWCNTs alongside their intrinsic E_{11} PL peak.[68] The study proposed that SWCNTs with smaller diameter readily oxidize during the dispersion process, which was corroborated by the reactions with H_2O_2.

In 2021, Xhylin and Ao investigated the photoreaction of SWCNTs dispersed in water in the presence of oxygen, forming oxidized SWCNTs.[69] The photoreaction was hindered when irradiated at wavelengths surpassing 300 nm irradiation and with specific dispersants. Particularly, the oxidation of SWCNTs proceeded efficiently when SDBS was used as a dispersion reagent. Conversely, oxidation was remarkably suppressed when DNA was employed for dispersion, given its higher reactivity toward reactive oxygen species compared to SWCNTs. These results indicate that the tuning of PL properties *via* oxidation can be modulated by UV irradiation and surfactant selection.

PL controlled by alkylation of SWCNTs

In 2013, Wang *et al.* reported the billups–Birch reductive alkylation of SWCNTs. This process involves the reaction of SWCNTs with sodium in liquid ammonia, followed by a reaction with 6-bromohexanoic acid. This resulted in a new PL peak at 1091 nm in the (6,5) SWCNTs with a smaller PL peak at 1225 nm (Scheme 2 and Fig. 4).[70] Their investigation indicated that the PL wavelengths were marginally influenced by the terminal groups, shifting to 1100 nm when the carboxylic acid was substituted by an amino group. The impact of alkylation on these properties was further validated by DFT calculations for
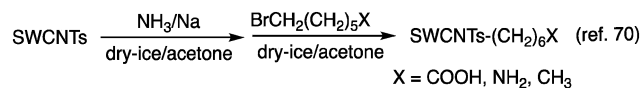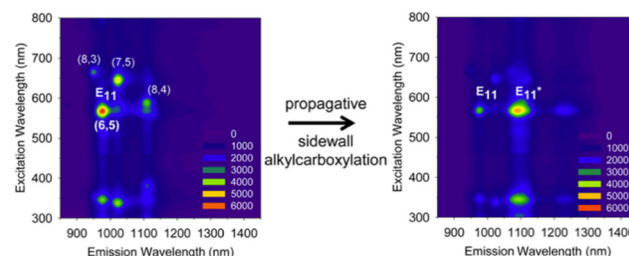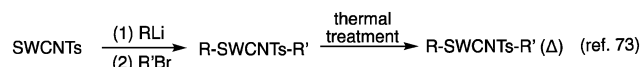
Scheme 2 Billup–Birch alkylation.

Fig. 4 Excitation–emission PL maps of SWCNTs-$(CH_2)_6$COOH dispersed in 1 wt% SDBS-D_2O. Reprinted with permission from ref. 70. Copyright 2014 American Chemical Society.

Scheme 3 Two-step alkylation and the subsequent thermal reaction.

1,4-methylated (6,5) SWCNTs, revealing a diminished HOMO–LUMO gap for 1,4-methylated (6,5) SWCNTs upon functionalization.

In 2015, Maeda *et al.* reported the stepwise alkylation of SWCNTs utilizing butyllithium and butyl bromide (Scheme 3).[71–73] No characteristic absorption and PL peaks were observed after butylation using *n*-butyllithium (*n*BuLi) and butyl bromide (*n*BuBr, *i*BuBr, *sec*BuBr, and *t*BuBr), owing to the highly efficient alkylation reaction. Conversely, the functionalization degree decreased when *t*-butyllithium (*t*BuLi) and *t*BuBr were used, resulting in a weak PL peak at approximately 1230 nm (E_{11}^{**} PL). To adjust the functionalization degree for other highly functionalized Bu-SWCNTs-Bu, thermal treatment was conducted under a nitrogen atmosphere. This was based on thermogravimetric (TG) analysis impeded by the functionalized SWCNTs, estimating their functionalization degree based on the observed weight losses. After thermal treatment of Bu-SWCNTs-Bu up to 300 °C, the E_{11}^{**} PL peak at ~1230 nm emerged with the recovery of the characteristic absorption and E_{11} PL peaks (Fig. 5). These results demonstrate the effectiveness of organolithium reagent functionalization and subsequent thermal treatment in selectively introducing a new PL peak at 1230 nm.

The functionalization degree of alkylated SWCNTs can be effectively reduced by considering the steric effects of the reagents, thermal treatment, and by changing the alkylation methods.[72,74] *n*-Butylated (6,5) SWCNTs ((6,5) SWCNTs-*n*Bu) prepared using sodium naphthalenide and *n*BuBr exhibited a lower functionalization degree than those prepared with butyllithium. Additionally, the former showed two new PL peaks at 1100 and 1230 nm (Fig. 6a–c). These PL wavelengths and their
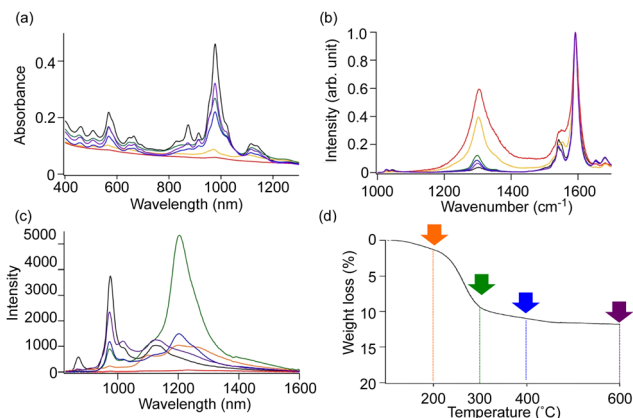
Fig. 5 (a) Absorption, (b) Raman, and (c) PL spectra of ^{t}Bu-SWCNTs-^{i}Bu before and after the thermal treatment. (d) TG curve of ^{t}Bu-SWCNTs-^{i}Bu. Black: ^{t}Bu-SWCNTs-^{i}Bu; orange: ^{t}Bu-SWCNTs-^{i}Bu (200 °C); green: ^{t}Bu-SWCNTs-^{i}Bu (300 °C); blue: ^{t}Bu-SWCNTs-^{i}Bu (400 °C); and purple: ^{t}Bu-SWCNTs-^{i}Bu (600 °C).

Fig. 6 (a) Absorption, (b) Raman, and (c) PL spectra of SWCNTs (black), ^{n}Bu-SWCNTs-Bu (red), ^{n}Bu-SWCNTs-^{n}Bu (300 °C) (green), and SWCNTs-^{n}Bu (blue). (d) Absorption and (e) PL spectra of SWCNTs (black), SWCNTs-xylyl (red), and SWCNTs-Bn (blue).

selectivities indicated that the structures and selectivities of the butylated SWCNTs differed based on the alkylation reagent. The time-resolved PL decay profiles of SWCNTs-^{n}Bu (200 °C) demonstrated that the PL peaks with a larger Stokes shift exhibited longer exciton lifetimes (E_{11} PL: 980 nm, ~23 ps. E_{11}^* PL: 1100 nm, ~65 ps. E_{11}^{**} PL: 1200 nm, ~118 ps.). In 2019, a time-resolved study of the PL decay of hexylated SWCNTs at 4.2 K identified two characteristic lifetimes for (6,5) E_{11} (τ_1 = 70 ps, τ_2 = 200 ps), E_{11}^* (τ_1 = 230 ps, τ_2 = 590 ps), and trion emission (τ_1 = 120 ps, τ_2 = 400 ps).[75] The efficacy of UCPL was confirmed using SWCNTs-^{n}Bu (200 °C), revealing increased UCPL efficiency at PL wavelengths with small Stokes shifts following functionalization.[49]

Benzylated (6,5) SWCNTs ((6,5) SWCNTs-Bn) prepared using benzyl bromide instead of bromobutane exhibited PL peaks at 1104 and 1197 nm. Conversely, the (6,5) SWCNT adduct prepared with 1,2-bis(bromomethyl)benzene ((6,5) SWCNTs-xylyl) selectively exhibited a new PL peak at 1231 nm (Fig. 6d and e).[49] In the fullerene C_{60} chemistry, reactions with benzyl bromide yielded both 1,2- and 1,4-adducts, whereas 1,2-bis(bromomethyl) benzene selectively yielded 1,2-adducts. These results indicate that the introduction of two reactive sites improves the selectivity of the binding configurations and the PL peak selectivity.

Ehara *et al.* reported DFT and TD-DFT calculations of the relative energies and HOMO–LUMO gaps of three 1,2- and three 1,4-adducts of model compounds of dialkylated SWCNTs and hydroalkylated SWCNTs with eight chiral angles.[76] Their work suggested that the selectivity of functionalization sites can be comprehended by the Clar sextet theory and cost-effective modeling. The binding configurations in the (6,5) SWCNT are denoted as 1,2-L_{87}, 1,2-L_{27}, 1,2-L_{-33}, 1,4-L_{87}, 1,4-L_{27}, and 1,4-L_{-33} (Fig. 7). The subscripts of L denote the positive or negative angles of two sp^3 carbon atoms on the SWCNTs relative to the SWCNT axis.[22] The 1,4-L_{87} adduct was the most stable for higher addenda bulkiness, whereas the 1,2-L_{-33} adduct was the most stable for lower addenda bulkiness. For instance, the
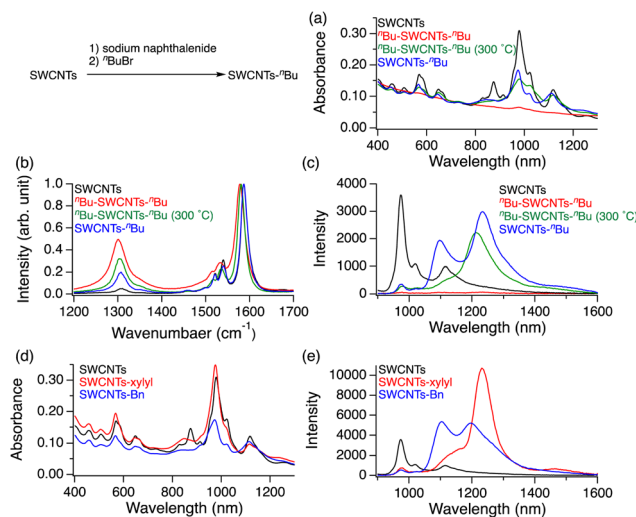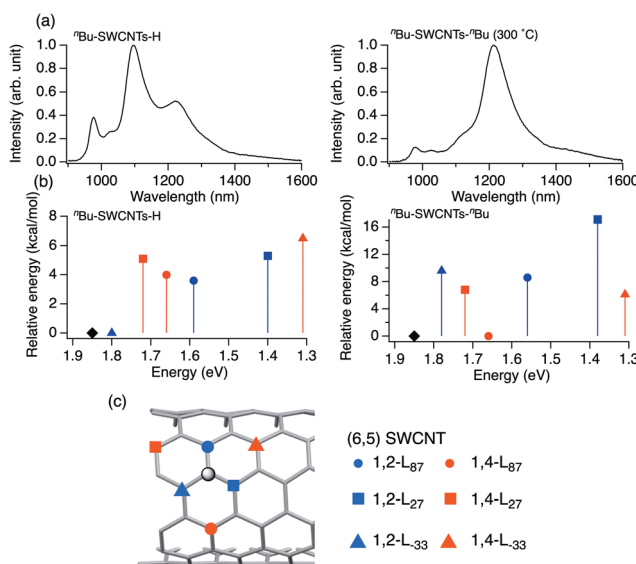

Fig. 7 (a) PL spectra of ^{n}Bu-SWCNTs-H (left) and ^{n}Bu-SWCNTs-^{n}Bu (300 °C) (right). (b) Energies (kcal mol^{-1}) of model ^{n}Bu-(6,5) SWCNT-H (left) and ^{n}Bu-(6,5) SWCNT-^{n}Bu (right) isomers plotted *versus* the calculated transition energy (eV). The 1,2- (blue) and 1,4-binding configurations (red) are classified according to their bond angles with respect to the SWCNT axis, marked as (●) L_{87}, (■) L_{27}, and (▲) L_{-33}. (◆): calculated transition energy of (6,5) SWCNTs. (c) Six different binding configurations relative to the central addition site (gray circles) are shown. (c) Six different binding configurations relative to the central addition site (gray circles) are shown. (c) Six binding configurations of 1,2- and 1,4-functionalized (6,5) SWCNTs. Reprinted with permission from ref. 48 and 76. Copyright 2023 American Chemical Society and Copyright 2019 American Chemical Society.

most stable binding configuration of ^{n}Bu-(6,5) SWCNTs-^{n}Bu is 1,4-L_{87}. When one of the addenda atoms was hydrogen, the 1,2-L_{-33} binding configuration was the most stable, regardless of

whether the other alkyl group was butyl or methyl. Building on these theoretical results, Maeda *et al.* prepared dialkylated and hydroalkylated SWCNT adducts (R-(6,5) SWCNTs-R and R-(6,5) SWCNTs-H) using alkyllithium (RLi, R = ^{n}Bu, Me), alkyl halide (^{n}BuBr, MeI), or trifluoroacetic acid. ^{n}Bu-SWCNTs-^{n}Bu exhibited a PL peak at 1230 nm, whereas Me-(6,5) SWCNTs-Me exhibited PL peaks at 1100 and 1230 nm.[48] A higher E_{11}^* PL intensity ratio relative to the E_{11}^{**} PL intensity was observed in Bu-(6,5) SWCNTs-H and Me-(6,5) SWNTs-H. The selectivity of the PL wavelength, depending on the reagents used, supported the relationship between the binding configurations and PL properties of the functionalized SWCNTs. Furthermore, the binding configurations could be controlled by the steric effects of the reagents.

In 2018, Maeda *et al.* explored the steric effects of reductive alkylation on SWCNT PL characteristics using first-, second-, and third-generation dendrons (**G1**, **G2**, and **G3**), molecules with repeating hyperbranched structures.[46] The functionalization degree decreased as the dendrons increased in bulkiness. Additionally, the intensity of the E_{11}^* PL peak at 1100 nm increased, while that of the E_{11}^{**} PL at 1230 nm decreased. These results suggest that steric repulsion of the reagents inhibited the 1,4-dialkylation reaction, favoring the 1,2-hydroalkylation reaction (Fig. 8). Theoretical calculations using the model molecules of hydroalkylated SWCNTs demonstrated that the 1,2-L$_{-33}$ adduct was the most stable isomer among the 1,2- and 1,4-adducts, irrespective of dendron generation. Furthermore, the transition energies remained almost unaffected across dendron generation. Therefore, sufficiently large-structured reactants enhance the hydroalkylation selectivity, promoting a 1100 nm PL peak from (6,5) SWCNTs. Wang *et al.* controlled the PL wavelength through steric hindrance in the arylation reactions with diazonium salts under acidic conditions.[43] By leveraging the steric hindrances of the aryl

groups and nucleophilic reagents, a new PL peak was observed in the 1130–1280 nm range from (6,5) SWCNTs.

In 2016, Wang *et al.* reported the tuning of the PL wavelength of (6,5) SWCNTs by alkylation in acetonitrile solution using alkyl halide, sodium bicarbonate, and sodium dithionate.[34] The PL wavelength of alkylated (6,5) SWCNTs was adjusted within the range of 1096–1158 nm by altering the number and positions of the fluorine atoms in the alkyl groups. For instance, the hexylated (6,5) SWCNTs and perfluorohexylated (6,5) SWCNTs displayed new PL peaks at 1096 and 1155 nm, respectively (Fig. 9). The 6,6,6-trifluorohexylated (6,5) SWCNTs and trifluoromethylated (6,5) SWCNTs exhibited new PL peaks at 1099 and 1158 nm, respectively. The linear correlation between the PL energy shift and calculated inductive constants (σ^*) of the fluoroalkyl groups indicates the role of inductive effects in dictating the PL wavelength (Table 2). Additionally, the calculated HOMO–LUMO gaps of the model compounds of trifluoromethylated (6,5) SWCNTs were smaller than those of the model compounds of methylated (6,5) SWCNTs, supporting a larger PL wavelength shift than that of the methylated (6,5) SWCNTs. The effects of monovalent and divalent chemical modifications were validated by comparison with SWCNT adducts functionalized with 1,2-diiodomethane, difluorodiiodomethane, and trifuluoroiodomethane, which exhibited new PL peaks at 1125, 1094, 1164, and 1158 nm, respectively. Divalent functionalization of the SWCNTs resulted in a new PL peak in the red-shifted region compared with the corresponding monovalent functionalization. Gifford *et al.*
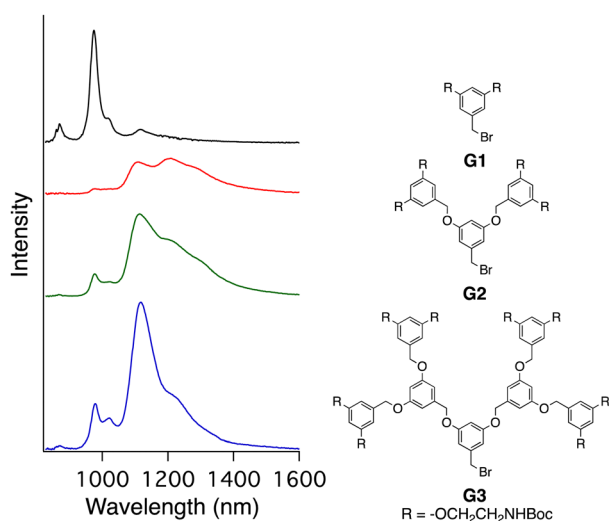

Fig. 8 PL spectra of SWCNTs (black) and dendron-functionalized SWCNTs (red: SWCNTs-**G1**; green: SWCNTs-**G2**; and blue: SWCNTs-**G3**). Dendron-functionalized SWCNTs were prepared using sodium naphthalenide and **G1**, **G2**, or **G3**.
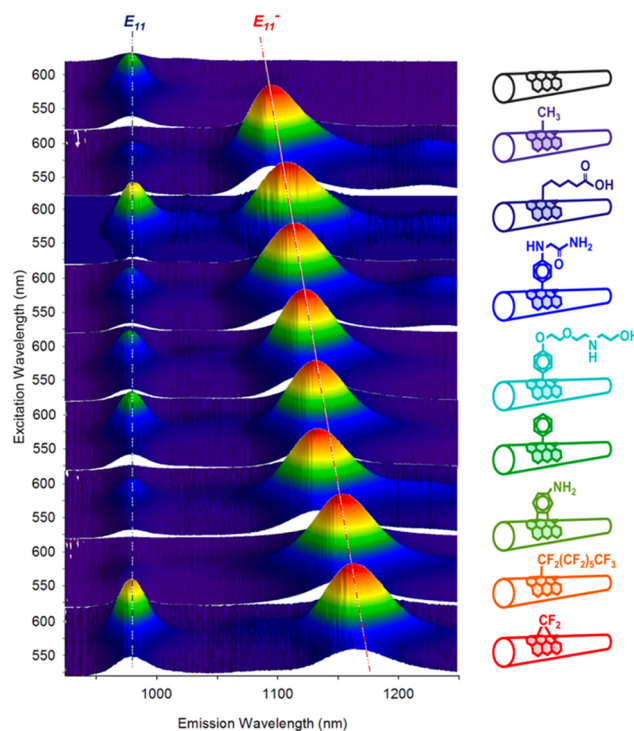

Fig. 9 Excitation–emission PL maps of the functionalized SWCNTs. Reprinted with permission from ref. 34. Copyright 2016 American Chemical Society.

Table 2 Spectral characteristics of alkylated and fluoroalkylated (6,5) SWCNTs and calculated inductive constants of the substituted alkyl and fluoroalkyl groups. -R and >R represent whether alkylating or fluoroalkylated reagents used is monoiodoalkane or diiodoalkane[34]

SWCNTs-R	E_{11}^* PL wavelength	σ^* (calcd.)
$-CH_2CH_2CH_2CH_2CH_2CH_3$	1096	−0.774
$-CH_2CH_2CH_2CH_2CH_2CF_3$	1099	−0.462
$-CH_2CH_2CH_2CH_2CF_2CF_3$	1107	−0.127
$-CH_2CH_2CF_2CF_2CF_2CF_3$	1137	1.086
$-CF_2CF_2CF_2CF_2CF_2CF_3$	1155	4.867
$-CH_2CH_2CH_2CH_2CF_3$	1104	−0.287
$-CH_2CH_2CH_2CF_3$	1101	−0.034
$-CH_2CH_2CF_3$	1110	0.310
$-CH_2CF_3$	1114	1.244
$-CF_3$	1158	3.961
$-CH_3$	1094	
$>CF_2$	1164	
$>CH_2$	1125	

conducted more comprehensive experimental and theoretical studies.[77] The theoretical calculations for the divalently functionalized SWCNTs (*e.g.*, SWCNT$>CH_2$) supported that inductive effects predominantly influence the PL wavelength, akin to monovalent functionalized SWCNTs (*e.g.*, 1,2-dimethylated SWCNT). Moreover, when juxtaposed with their monovalent counterparts, the divalently functionalized SWCNTs manifested a significant 's' character at the binding carbon atoms on SWCNTs, underpinning the emergence of a stronger red-shifted PL peak.

He *et al.* demonstrated the $[2\pi + 2\pi]$ photocycloaddition of SWCNTs with enones, resulting in new PL peaks from (6,5) SWCNTs at 1114 and 1255 nm (Fig. 10).[78] The reaction proceeded upon 285 or 566 nm irradiation and was inhibited by a radical scavenger, suggesting an electron transfer mechanism *via* the excited state of the SWCNTs or enone. DFT calculations of the corresponding model compounds of the $[2\pi + 2\pi]$, $[2\pi + 4\pi]$, and $[4\pi + 2\pi]$ cycloaddition products were performed. The results indicated that the $[2\pi + 2\pi]$ cycloaddition product is a thermodynamically favored structure. The binding configuration and interaction between the SWCNT surface and the side chains of the addenda were also confirmed, underscoring the significance of dispersion interactions and steric effects on chemo- and regioselectivity.

Maeda *et al.* investigated the functionalization of (6,5) SWCNTs using sodium naphthalenide and 1,*n*-dibromoalkane (*n* = 3–5). They observed selective new PL peaks at 1215 (*n* = 3), 1230 (*n* = 4), and 1231 nm (*n* = 5).[50] However, employing the corresponding monobromoalkane instead of dibromoalkane induced two new PL peaks at approximately 1100 and 1230 nm (Fig. 11, left). Theoretical calculations of the model compounds for cyclic addition products affirmed that the PL peak variations correlated with alkyl chain length. These calculations showed that both the transition energy and sum of the bond angles at the addition sites increased with increasing alkyl chain length. No similar relationship between the chain length and transition energy was observed for the functionalized SWCNTs with propyl bromide and butyl bromide. This suggests that 1,*n*-dibromoalkanes (*n* = 3–5) lead to
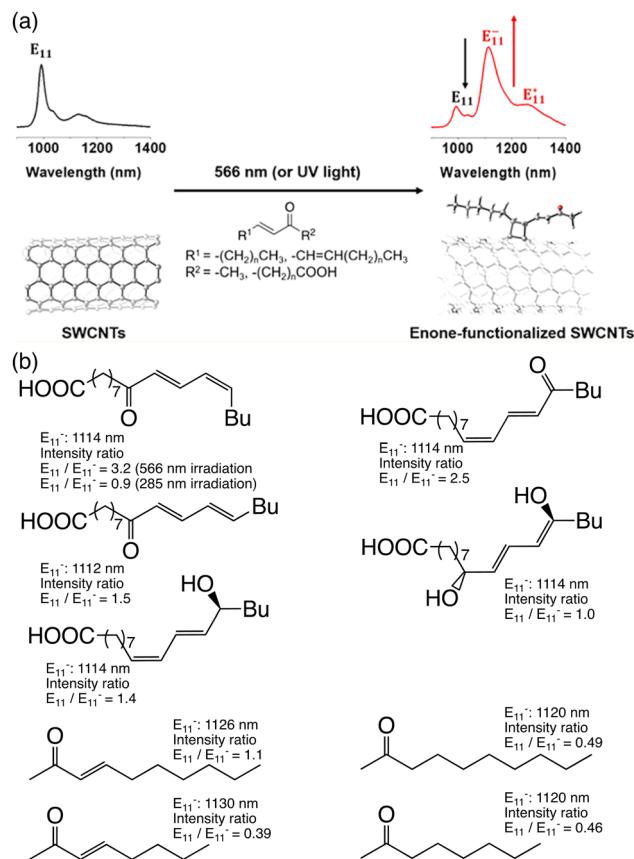

Fig. 10 (a) Reaction scheme of the photoreaction of SWCNTs with enones, PL spectra, and computed structure of enone-functionalized SWCNTs. (b) Structure of enones, PL wavelength of enone-functionalized SWCNTs, and E_{11}^- PL intensity ratio toward the E_{11} PL peak after 1 h of irradiation at 566 nm. Reprinted with permission from ref. 78. Copyright 2021 American Chemical Society.

cycloaddition products that selectively yield a new PL peak. This selective emergence of new PL peaks does not occur when the alkyl chain length is 6 or more (Fig. 11, right).[50,52] The most stable 1,2-addition product of (6,5) SWCNTs-C_nH_{2n} (*n* = 3–5) was the 1,2-L$_{-33}$ binding configuration, which is the same binding configuration observed for hydroalkylated (6,5) SWCNTs. From the comparison of the experimentally observed PL wavelength, calculated transition energy, and relative stability, the thermodynamically favored 1,2-L$_{-33}$ binding configuration was excluded as a plausible candidate for the cycloaddition products. The functionalization of (6,5) SWCNTs using 2,4-dibromopentane (SWCNTs-$C_3H_4Me_2$) led to a new PL peak at 1216 nm. Additionally, after thermal treatment for 6 h (SWCNTs-$C_3H_4Me_2$(300 °C, 6 h)), a new PL peak emerged at 1268 nm, while the intensity of the PL peak at 1216 nm decreased (Fig. 12).[51] As a potential explanation for this shift in the PL characteristics is the thermal rearrangement of the 1,2-L$_{87}$ adduct to the more stable 1,2-L$_{27}$ adduct. The spin density of the butylated (6,5) SWCNT radical (SWCNT-^nBu radical) is higher at the 1,2-L$_{87}$ carbon atom than at the 1,2-L$_{-33}$ carbon atom, suggesting that the 1,2-L$_{87}$ binding configuration is kinetically preferred.
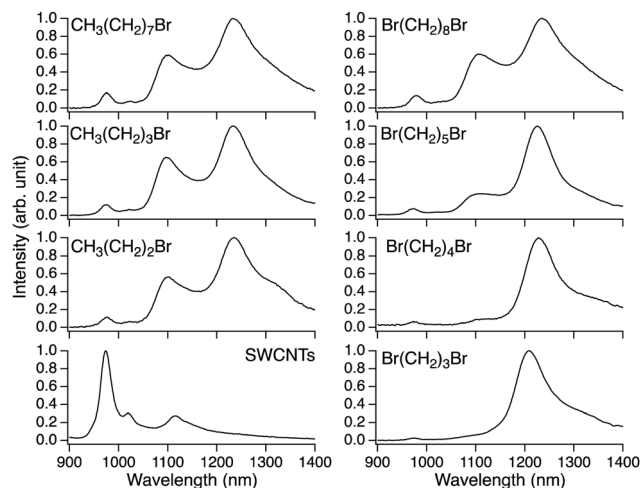
Fig. 11 PL spectra of SWCNTs and alkylated SWCNTs using sodium naphthalenide and bromoalkene or 1,*n*-dibromoalkane. The reagents used are shown in the PL spectra.
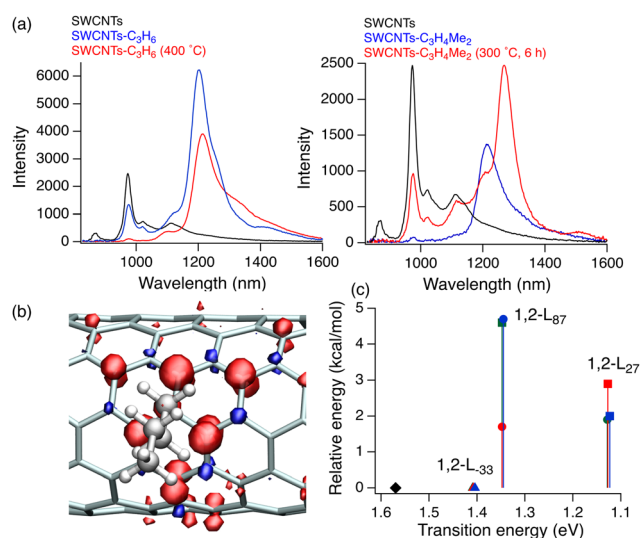

Fig. 12 (a) PL spectra of SWCNTs, SWCNTs-C_3H_6, SWCNTs-C_3H_6 (300 °C), SWCNTs-$C_3H_4Me_2$, and SWCNTs-$C_3H_4Me_2$ (300 °C, 6 h). (b) Calculated spin density distribution (isovalue = 0.004) of the (6,5) SWCNT-^nBu radical at the B3LYP/6-31G* level. 1,2-L_{-33}: 0.2116; 1,2-L_{27}: 0.1479; 1,2-L_{87}: 0.2121, 1,4-L_{-33}: 0.1849; 1,4-L_{27}: 0.1220; 1,4-L_{87}: 0.1623. (c) Calculated transition energy (in eV) and relative energies (kcal mol^{-1}) of the model molecules of (6,5) SWCNT-C_3H_6 (green), (6,5) *cis*-SWCNT-$C_3H_4Me_2$ (red), and (6,5) *trans*-SWCNT-$C_3H_4Me_2$ (blue).

Shiraki *et al.* reported an arylation reaction using two aryldiazonium reagents linked by alkyl chains to produce new PL peaks at longer wavelengths than those of SWCNT adducts prepared using the corresponding single aryldiazonium salts.[26,27]

In 2023, Maeda *et al.* reported that (6,5) SWCNTs exhibited a PL peak at 1320 nm when the cycloaddition reaction was influenced by the electronic effect of fluorine atoms (Fig. 13).[42] The reductive perfluorobutylation of (6,5) SWCNTs using sodium naphthalenide and 1,1,2,2,3,3,4,4,4-nonafluoro-1-iodobutane ($CF_3CF_2CF_2CF_2I$) resulted in a new PL peak selectively at 1152 nm. However,
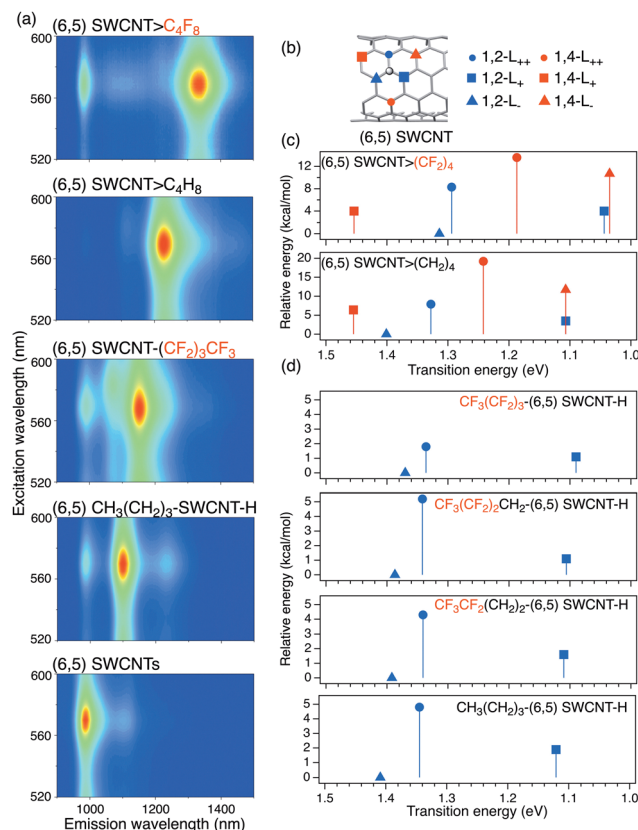

Fig. 13 (a) PL excitation–emission maps of SWCNTs and functionalized SWCNTs reagents: $C_4F_8I_2$, $C_4H_8Br_2$, C_4F_9I, and C_4H_9Br. (b) Six binding configurations of the (6,5) SWCNTs. (c) and (d) Calculated transition energies (eV) and relative energies (in kcal mol^{-1}) of model molecules of the functionalized (6,5) SWCNTs. Reprinted with permission from ref. 42. Copyright 2023 Springer Nature.

butylation using 1-bromobutane produced new PL peaks at 1100 and 1230 nm. It was proposed that hydroperfluoroalkylation proceeded selectively under these reaction conditions, resulting in one PL peak at 1152 nm owing to the low functionalization degree compared to the corresponding butylation. Furthermore, the PL selectivity was strongly influenced by the number and position of fluorine atoms in iodobutane. In the reaction using 1,1,2,2,3,3,4,4-octafluoro-1,4-diiodobutane, a new PL peak emerged at 1320 nm for (6,5) SWCNTs. Therefore, it was proposed that the cycloaddition reaction proceeds efficiently using perfluorodiiodo-butane owing to the stereoelectronic effect. Theoretical calculations of the model molecules showed that octafluorobutylated (6,5) SWCNTs possess lower transition energies than the corresponding butylated (6,5) SWCNTs in identical 1,2- and 1,4-binding config-urations. Replacing hydrogen atoms with fluorine atoms in the alkylated SWCNTs lowers the LUMO energy.

PL characteristics of oxidized and alkylated SWCNTs with other chirality

As shown in Fig. 1b and c, the selective utilization of specific (*n*,*m*) SWCNTs expands their potential as PL materials

Table 3 Selected PL wavelengths of functionalized (n,m) SWCNTs

(n,m)	(7,3)	(6,4)	(9,1)	(6,5)	(8,3)	(9,2)	(7,5)	(8,4)
SWCNTs-O[20]	889	1012	924	983	960	1147	1033	1125
SWCNTs-C$_6$H$_4$NO$_2$[24]		1058		1137	1154	1300	1179	1263
^{n}Bu-SWCNTs-H[48]	1128, 1213	1015		1104, 1231	1160		1237	
SWCNTs-C$_4$F$_9$[42]	1185	1068	1153	1152	1164		1178	
^{n}Bu-SWCNTs-^{n}Bu (300 °C)[48]	1251	1119		1213	1160		1237	
SWCNTs-C$_3$H$_6$[52]	1251	1101		1215	1146		1231	1339
SWCNTs-C$_4$H$_8$[52]	1265	1115		1229	1170		1248	
SWCNTs-C$_3$H$_4$Me$_2$[47,51]	1249	1098, 1192		1213	1151, 1251		1234, 1310	1337
SWCNTs-C$_3$H$_4$Me$_2$ (300 °C, 6 h)[47,51]	1252, 1317	1104, 1174		1268	1146, 1255		1298	
SWCNTs-C$_4$F$_8$[42]	1373	1064, 1222	1207	1320	1269	1345		

at various excitation and emission wavelengths. Chemical functionalization has diversified the excitation spectrum for (6,5) SWCNTs, introducing 980 nm alongside 567 nm, and the emission wavelength was extended up to 1320 nm. Beyond (6,5) SWCNTs, research has delved into the oxidation,[20] arylation,[24,29,32,33,43,44,79] and alkylation[42,48,52,80] of separated (n,m) SWCNTs, and the separation of functionalized (n,m) SWCNTs, to elucidate the impact of functionalization on their PL properties. The separation of functionalized SWCNTs was conducted using SWCNT separation methods.[81,82] These studies have broadly expanded the excitation and emission wavelengths for various applications. A distinct (n,m)-dependent reactivity has been clarified in the arylation reaction.[37,79] Table 3 and Fig. 14 show the selected PL wavelengths of the functionalized SWCNTs with different chiral indices. Furthermore, the optical resolution of the functionalized SWCNTs has been achieved for (6,5) chirality.[42,48,52,80]

The functionalization of (6,5) SWCNTs using 2,4-dibromopentane to produce SWCNTs-C$_3$H$_4$Me$_2$ led to a new PL peak at 1216 nm. The subsequent thermal treatment produced a new PL peak at 1268 nm, SWCNTs-C$_3$H$_4$Me$_2$(300 °C, 6 h), while the intensity of the PL peak at 1216 nm decreased (Fig. 12).[51] The chiral separation of SWCNTs-C$_3$H$_4$Me$_2$(300 °C, 6 h)[41] revealed that a new PL peak at the red-shifted wavelength also emerged in (7,3) and (6,5) SWCNTs-C$_3$H$_4$Me$_2$(300 °C, 6 h) at 1317 and 1268 nm. The (6,4), (8,3), and (7,5) SWCNTs-C$_3$H$_4$Me$_2$ exhibited two new PL peaks at red-shifted wavelengths even without thermal treatment: (6,4) at 1098 and 1174 nm, (8,3) at 1151 and 1251 nm, and (7,5) at 1234 and 1310 nm. For the (8,3), (7,5), and (8,4) SWCNT adducts, the elimination reaction proceeded preferentially after thermal treatment. These results suggest that the binding configuration can be controlled by the substituent effect of the cyclic addenda and that thermal rearrangement and elimination reactions might compete depending on the chiral indices of SWCNTs.

Conclusion and outlook

In summary, the chemical functionalization of SWCNTs is a powerful tool for controlling PL characteristics, such as wavelength and efficiency. Fine-tuning the PL wavelength to improve efficiency is expected to expand the applicability of NIR light-emitting materials and extend their range of applications in bioimaging and optical communications. The insights obtained from the arylation, oxidation, and alkylation of the SWCNTs are mutually beneficial and contribute to a better understanding of the PL wavelength control over a wide range. Systematic theoretical calculations using model compounds have provided insights into the determinants of the PL wavelength. Estimations of the binding configurations of the functionalized SWCNTs were deduced by juxtaposing the PL wavelengths with theoretical computation outcomes. These results provide crucial guidance for the design and synthesis of functional SWCNTs. Further control of SWCNT PL wavelengths and determination of the binding configuration of the SWCNT adducts are expected in the near future.

Author contributions

Y. M. wrote the manuscript. Y. M., P. Z., and M. E. discussed and revised the manuscript. All authors approved the final version of the manuscript.
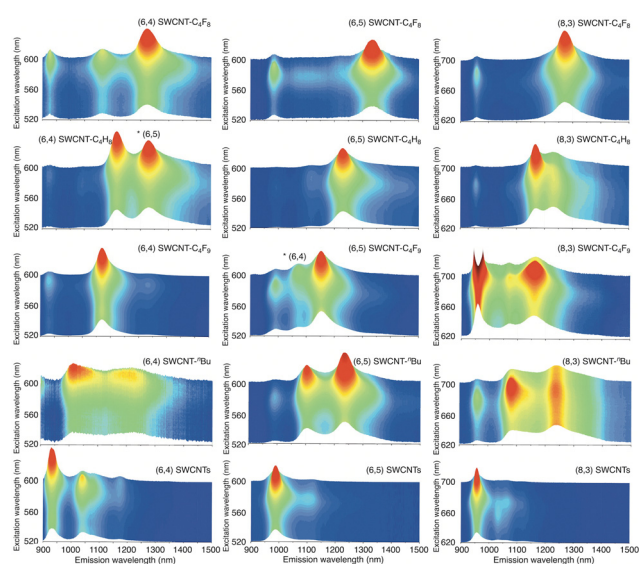

Fig. 14 (a) Excitation−emission PL maps of (6,4), (6,5), and (8,3) SWCNTs and functionalized SWCNTs. Reprinted with permission from ref. 42. Copyright 2023 Springer Nature.

Conflicts of interest

There are no conflicts to declare.

Acknowledgements

Notes and references

1 S. Iijima and T. Ichihashi, *Nature*, 1993, **363**, 603–605.
2 D. S. Bethune, C. H. Kiang, M. S. de Vries, G. Gorman, R. Savoy, J. Vazquez and R. Beyers, *Nature*, 1993, **363**, 605–607.
3 R. Saito, M. Fujita, G. Dresselhaus and M. S. Dresselhaus, *Appl. Phys. Lett.*, 1992, **60**, 2204–2206.
4 S. M. Bachilo, M. S. Strano, C. Kittrell, R. H. Hauge, R. E. Smalley and R. B. Weisman, *Science*, 2002, **298**, 2361–2366.
5 A. M. Rao, E. Richter, S. Bandow, B. Chase, P. C. Eklund, K. A. Williams, S. Fang, K. R. Subbaswamy, M. Menon, A. Thess, R. E. Smalley, G. Dresselhaus and M. S. Dresselhaus, *Science*, 1997, **275**, 187–191.
6 M. J. O'Connell, S. M. Bachilo, C. B. Huffman, V. C. Moore, M. S. Strano, E. H. Haroz, K. L. Rialon, P. J. Boul, W. H. Noon, C. Kittrell, J. Ma, R. H. Hauge, R. B. Weisman and R. E. Smalley, *Science*, 2002, **297**, 593–596.
7 P. Nikolaev, M. J. Bronikowski, R. K. Bradley, F. Rohmund, D. T. Colbert, K. A. Smith and R. E. Smalley, *Chem. Phys. Lett.*, 1999, **313**, 91–97.
8 Y. Maeda, S. I. Kimura, Y. Hiroshima, M. Kanda, Y. Lian, T. Wakahara, T. Akasaka, T. Hasegawa, H. Tokumoto, T. Shimizu, H. Kataura, Y. Miyauchi, S. Maruyama, K. Kobayashi and S. Nagase, *J. Phys. Chem. B*, 2004, **108**, 18395–18397.
9 Y. Maeda, S. I. Kimura, M. Kanda, Y. Hirashima, T. Hasegawa, T. Wakahara, Y. Lian, T. Nakahodo, T. Tsuchiya, T. Akasaka, J. Lu, X. Zhang, Z. Gao, Y. Yu, S. Nagase, S. Kazaoui, N. Minam, T. Shimizu, H. Tokumoto and R. Saito, *J. Am. Chem. Soc.*, 2005, **127**, 10287–10290.
10 Y. Maeda, M. Kanda, M. Hashimoto, T. Hasegawa, S. I. Kimura, Y. Lian, T. Wakahara, T. Akasaka, S. Kazaoui, N. Minami, T. Okazaki, Y. Hayamizu, K. Hata, J. Lu and S. Nagase, *J. Am. Chem. Soc.*, 2006, **128**, 12239–12242.
11 A. Nish, J. Y. Hwang, J. Doig and R. J. Nicholas, *Nat. Nanotechnol.*, 2007, **2**, 640–646.
12 Y. Maeda, T. Kato, J. Higo, T. Hasegawa, T. Kitano, T. Tsuchiya, T. Akasaka, T. Okazaki, J. Lu and S. Nagase, *NANO*, 2008, **3**, 455–459.
13 A. Nish, J. Y. Hwang, J. Doig and R. J. Nicholas, *Nanotechnology*, 2008, **19**, 095603.
14 A. A. Boghossian, J. Zhang, P. W. Barone, N. F. Reuel, J. H. Kim, D. A. Heller, J. H. Ahn, A. J. Hilmer, A. Rwei, J. R. Arkalgud, C. T. Zhang and M. S. Strano, *ChemSusChem*, 2011, **4**, 848–863.
15 T. Endo, J. Ishi-Hayase and H. Maki, *Appl. Phys. Lett.*, 2015, **106**, 113106.
16 J. A. Thomas, *Chem. Soc. Rev.*, 2015, **44**, 4494–4500.
17 J. Li and K. Pu, *Chem. Soc. Rev.*, 2019, **48**, 38–71.
18 J. Crochet, M. Clemens and T. Hertel, *J. Am. Chem. Soc.*, 2007, **129**, 8058–8059.
19 X. Wei, T. Tanaka, S. Li, M. Tsuzuki, G. Wang, Z. Yao, L. Li, Y. Yomogida, A. Hirano, H. Liu and H. Kataura, *Nano Lett.*, 2020, **20**, 410–417.
20 S. Ghosh, S. M. Bachilo, R. A. Simonette, K. M. Beckingham and R. B. Weisman, *Science*, 2010, **330**, 1656–1659.
21 Y. Miyauchi, M. Iwamura, S. Mouri, T. Kawazoe, M. Ohtsu and K. Matsuda, *Nat. Photonics*, 2013, **7**, 715–719.
22 X. He, B. J. Gifford, N. F. Hartmann, R. Ihly, X. Ma, S. V. Kilina, Y. Luo, K. Shayan, S. Strauf, J. L. Blackburn, S. Tretiak, S. K. Doorn and H. Htoon, *ACS Nano*, 2017, **11**, 10785–10796.
23 B. J. Gifford, S. Kilina, H. Htoon, S. K. Doorn and S. Tretiak, *J. Phys. Chem. C*, 2017, **122**, 1828–1838.
24 Y. Piao, B. Meany, L. R. Powell, N. Valley, H. Kwon, G. C. Schatz and Y. Wang, *Nat. Chem.*, 2013, **5**, 840–845.
25 J. Zhang, M. P. Landry, P. W. Barone, J. H. Kim, S. Lin, Z. W. Ulissi, D. Lin, B. Mu, A. A. Boghossian, A. J. Hilmer, A. Rwei, A. C. Hinckley, S. Kruss, M. A. Shandell, N. Nair, S. Blake, F. Sen, S. Sen, R. G. Croy, D. Li, K. Yum, J. H. Ahn, H. Jin, D. A. Heller, J. M. Essigmann, D. Blankschtein and M. S. Strano, *Nat. Nanotechnol.*, 2013, **8**, 959–968.
26 T. Shiraki, T. Shiraishi, G. Juhasz and N. Nakashima, *Sci. Rep.*, 2016, **6**, 28393.
27 T. Shiraki, B. Yu, T. Shiraishi, T. Shiga and T. Fujigaya, *Chem. Lett.*, 2019, **48**, 791–794.
28 F. J. Berger, J. Lüttgens, T. Nowack, T. Kutsch, S. Lindenthal, L. Kistner, C. C. Müller, L. M. Bongartz, V. A. Lumsargis, Y. Zakharko and J. Zaumseil, *ACS Nano*, 2019, **13**, 9259–9269.
29 H. B. Luo, P. Wang, X. Wu, H. Qu, X. Ren and Y. Wang, *ACS Nano*, 2019, **13**, 8417–8424.
30 X. Wu, M. Kim, H. Kwon and Y. Wang, *Angew. Chem., Int. Ed.*, 2018, **57**, 648–653.
31 Y. Zheng, S. M. Bachilo and R. B. Weisman, *ACS Nano*, 2020, **14**, 715–723.
32 S. Settele, F. J. Berger, S. Lindenthal, S. Zhao, A. A. El Yumin, N. F. Zorn, A. Asyuda, M. Zharnikov, A. Hogele and J. Zaumseil, *Nat. Commun.*, 2021, **12**, 2119.
33 Y. Zheng, Y. Han, B. M. Weight, Z. Lin, B. J. Gifford, M. Zheng, D. Kilin, S. Kilina, S. K. Doorn, H. Htoon and S. Tretiak, *Nat. Commun.*, 2022, **13**, 4439.
34 H. Kwon, A. Furmanchuk, M. Kim, B. Meany, Y. Guo, G. C. Schatz and Y. Wang, *J. Am. Chem. Soc.*, 2016, **138**, 6878–6885.
35 D. Kozawa, X. Wu, A. Ishii, J. Fortner, K. Otsuka, R. Xiang, T. Inoue, S. Maruyama, Y. Wang and Y. K. Kato, *Nat. Commun.*, 2022, **13**, 2814.
36 L. R. Powell, M. Kim and Y. Wang, *J. Am. Chem. Soc.*, 2017, **139**, 12533–12540.
37 A. H. Brozena, M. Kim, L. R. Powell and Y. Wang, *Nat. Rev. Chem.*, 2019, **3**, 375–392.
38 B. J. Gifford, S. Kilina, H. Htoon, S. K. Doorn and S. Tretiak, *Acc. Chem. Res.*, 2020, **53**, 1791–1801.
39 T. Shiraki, Y. Miyauchi, K. Matsuda and N. Nakashima, *Acc. Chem. Res.*, 2020, **53**, 1846–1859.
40 D. Janas, *Mater. Horiz.*, 2020, **7**, 2860–2881.
41 J. Zaumseil, *Adv. Opt. Mater.*, 2021, **10**, 2101576.
42 Y. Maeda, M. Suzuki, Y. Konno, P. Zhao, N. Kikuchi, M. Yamada, M. Mitsuishi, A. T. N. Dao, H. Kasai and M. Ehara, *Commun. Chem.*, 2023, **6**, 159.
43 P. Wang, J. Fortner, H. Luo, J. Klos, X. Wu, H. Qu, F. Chen, Y. Li and Y. Wang, *J. Am. Chem. Soc.*, 2022, **144**, 13234–13241.
44 B. Yu, S. Naka, H. Aoki, K. Kato, D. Yamashita, S. Fujii, Y. K. Kato, T. Fujigaya and T. Shiraki, *ACS Nano*, 2022, **16**, 21452–21461.
45 B. Yu, T. Fujigaya and T. Shiraki, *Bull. Chem. Soc. Jpn.*, 2023, **96**, 127–132.
46 Y. Maeda, Y. Konno, M. Yamada, P. Zhao, X. Zhao, M. Ehara and S. Nagase, *Nanoscale*, 2018, **10**, 23012–23017.
47 Y. Maeda, R. Morooka, P. Zhao, M. Yamada and M. Ehara, *Chem. Commun.*, 2023, **59**, 11648–11651.
48 Y. Maeda, R. Morooka, P. Zhao, D. Uchida, Y. Konno, M. Yamada and M. Ehara, *J. Phys. Chem. C*, 2023, **127**, 2360–2370.
49 Y. Maeda, S. Minami, Y. Takehana, J. S. Dang, S. Aota, K. Matsuda, Y. Miyauchi, M. Yamada, M. Suzuki, R. S. Zhao, X. Zhao and S. Nagase, *Nanoscale*, 2016, **8**, 16916–16921.
50 Y. Maeda, K. Kuroda, H. Tambo, H. Murakoshi, Y. Konno, M. Yamada, P. Zhao, X. Zhao, S. Nagase and M. Ehara, *RSC Adv.*, 2019, **9**, 13998–14003.
51 Y. Maeda, H. Murakoshi, H. Tambo, P. Zhao, K. Kuroda, M. Yamada, X. Zhao, S. Nagase and M. Ehara, *Chem. Commun.*, 2019, **55**, 13757–13760.
52 Y. Konno, R. Morooka, T. Morishita, P. Zhao, N. Miyasaka, K. Ono, A. Noda, D. Uchida, R. Iwasaki, M. Yamada, M. Ehara and Y. Maeda, *Chem. – Eur. J.*, 2023, **29**, e202300766.
53 N. Akizuki, S. Aota, S. Mouri, K. Matsuda and Y. Miyauchi, *Nat. Commun.*, 2015, **6**, 8920.
54 R. B. Weisman and S. M. Bachilo, *Nano Lett.*, 2003, **3**, 1235–1238.

55 H. Telg, J. Maultzsch, S. Reich and C. Thomsen, *Phys. Rev. B: Condens. Matter Mater. Phys.*, 2006, **74**, 115415.

56 M. S. Strano, S. K. Doorn, E. H. Haroz, C. Kittrell, R. H. Hauge and R. E. Smalley, *Nano Lett.*, 2003, **3**, 1091–1096.

57 X. Ma, L. Adamska, H. Yamaguchi, S. E. Yalcin, S. Tretiak, S. K. Doorn and H. Htoon, *ACS Nano*, 2014, **8**, 10782–10789.

58 Y. Iizumi, M. Yudasaka, J. Kim, H. Sakakita, T. Takeuchi and T. Okazaki, *Sci. Rep.*, 2018, **8**, 6272.

59 Y. Maeda, Y. Niino, T. Kondo, M. Yamada, T. Hasegawa and T. Akasaka, *Chem. Lett.*, 2011, **40**, 1431–1433.

60 Y. Maeda, J. Higo, Y. Amagai, J. Matsui, K. Ohkubo, Y. Yoshigoe, M. Hashimoto, K. Eguchi, M. Yamada, T. Hasegawa, Y. Sato, J. Zhou, J. Lu, T. Miyashita, S. Fukuzumi, T. Murakami, K. Tohji, S. Nagase and T. Akasaka, *J. Am. Chem. Soc.*, 2013, **135**, 6356–6362.

61 C. F. Chiu, W. A. Saidi, V. E. Kagan and A. Star, *J. Am. Chem. Soc.*, 2017, **139**, 4859–4865.

62 C. W. Lin, S. M. Bachilo, Y. Zheng, U. Tsedev, S. Huang, R. B. Weisman and A. M. Belcher, *Nat. Commun.*, 2019, **10**, 2874.

63 T. Eremin, V. Eremina, Y. Svirko and P. Obraztsov, *Nanomaterials*, 2023, **13**, 1561.

64 M. Yang, T. Okazaki and M. Zhang, *Toxics*, 2021, **9**, 223.

65 Y. Maeda, Y. Konno, A. Nishino, M. Yamada, S. Okudaira, Y. Miyauchi, K. Matsuda, J. Matsui, M. Mitsuishi and M. Suzuki, *Nanoscale*, 2020, **12**, 6263–6270.

66 Y. Tan and D. E. Resasco, *J. Phys. Chem. B*, 2005, **109**, 14454–14460.

67 E. Manousaki, E. Psillakis, N. Kalogerakis and D. Mantzavinos, *Water Res.*, 2004, **38**, 3751–3759.

68 X. Wei, T. Tanaka, N. Akizuki, Y. Miyauchi, K. Matsuda, M. Ohfuchi and H. Kataura, *J. Phys. Chem. C*, 2016, **120**, 10705–10710.

69 F. Xhyliu and G. Ao, *J. Phys. Chem. C*, 2021, **125**, 9236–9243.

70 Y. Zhang, N. Valley, A. H. Brozena, Y. Piao, X. Song, G. C. Schatz and Y. Wang, *J. Phys. Chem. Lett.*, 2013, **4**, 826–830.

71 Y. Maeda, T. Kato, T. Hasegawa, M. Kako, T. Akasaka, J. Lu and S. Nagase, *Org. Lett.*, 2010, **12**, 996–999.

72 Y. Maeda, K. Saito, N. Akamatsu, Y. Chiba, S. Ohno, Y. Okui, M. Yamada, T. Hasegawa, M. Kako and T. Akasaka, *J. Am. Chem. Soc.*, 2012, **134**, 18101–18108.

73 Y. Maeda, Y. Takehana, M. Yamada, M. Suzuki and T. Murakami, *Chem. Commun.*, 2015, **51**, 13462–13465.

74 Y. Maeda, Y. Takehana, J. S. Dang, M. Suzuki, M. Yamada and S. Nagase, *Chem. – Eur. J.*, 2017, **23**, 1789–1794.

75 M. Nutz, J. Zhang, M. Kim, H. Kwon, X. Wu, Y. Wang and A. Hogele, *Nano Lett.*, 2019, **19**, 7078–7084.

76 P. Zhao, Y. Maeda and M. Ehara, *J. Phys. Chem. C*, 2019, **123**, 18629–18637.

77 B. J. Gifford, X. He, M. Kim, H. Kwon, A. Saha, A. E. Sifain, Y. Wang, H. Htoon, S. Kilina, S. K. Doorn and S. Tretiak, *Chem. Mater.*, 2019, **31**, 6950–6961.

78 X. He, I. Kevlishvili, K. Murcek, P. Liu and A. Star, *ACS Nano*, 2021, **15**, 4833–4844.

79 A. Saha, B. J. Gifford, X. He, G. Ao, M. Zheng, H. Kataura, H. Htoon, S. Kilina, S. Tretiak and S. K. Doorn, *Nat. Chem.*, 2018, **10**, 1089–1095.

80 Y. Maeda, Y. Konno and M. Yamada, *J. Phys. Chem. C*, 2020, **124**, 21886–21894.

81 X. Wei, S. Li, W. Wang, X. Zhang, W. Zhou, S. Xie and H. Liu, *Adv. Sci.*, 2022, **9**, e2200054.

82 D. Janas, *Mater. Chem. Front.*, 2018, **2**, 36–63.